Role of magnetic field curvature in magnetohydrodynamic turbulence

Yan Yang (iD), Minping Wan, William H. Matthaeus (iD), Yipeng Shi, Tulasi N. Parashar, Quanming Lu, and Shiyi Chen (iD)

View Online   Export Citation   CrossMark

ARTICLES YOU MAY BE INTERESTED IN

Role of magnetic field curvature in magnetohydrodynamic turbulence

View Online   Export Citation   CrossMark

Yan Yang,[1,2] (iD) Minping Wan,[1,a)] William H. Matthaeus,[3] (iD) Yipeng Shi,[4] Tulasi N. Parashar,[3] Quanming Lu,[2] and Shiyi Chen[1] (iD)

AFFILIATIONS

[1]Southern University of Science and Technology, Shenzhen, Guangdong 518055, China
[2]University of Science and Technology of China, Hefei, Anhui 230026, China
[3]University of Delaware, Newark, Delaware 19716, USA
[4]Peking University, Beijing 100871, China

[a)]Electronic mail: wanmp@sustech.edu.cn

ABSTRACT

Magnetic fields are transported and tangled by turbulence, even as they lose identity due to nonideal or resistive effects. In a balanced field, lines undergo stretch-twist-fold processes. The curvature field, a scalar that measures the tangling of the magnetic field lines, is studied in detail here, in the context of magnetohydrodynamic turbulence. A central finding is that the magnitudes of curvature and magnetic field are anticorrelated. A high curvature colocates with a low magnetic field, which gives rise to power-law tails of the probability density function of the curvature field. The curvature drift term that converts magnetic energy into flow and thermal energy largely depends on the curvature field behavior, a relationship that helps to explain particle acceleration due to the curvature drift. This adds as well to evidence that turbulent effects most likely play an essential role in particle energization since turbulence drives stronger tangled field configurations, and therefore curvature.

Published under license by AIP Publishing. https://doi.org/10.1063/1.5099360

I. INTRODUCTION

A divergence-free vector field, such as the magnetic field, can be conveniently visualized in terms of field lines, which are tangent to the field everywhere. In many astrophysical and space plasmas, magnetic field lines play an essential role, in general for describing the topology and connectivity at a single instance of time, and even for developing theoretical descriptions of dynamical processes such as magnetic reconnection.[1] Magnetic field lines are also widely used in describing mechanisms for particle acceleration and for the transport of suprathermal and energetic particles. Ambiguities in defining field lines, especially as a function of time, are well known.[2] In turbulence, magnetic field lines are in general not well-ordered, but rather exhibit complex structures and wander randomly in space.[3–5] Moving into the realm of magnetic reconnection, the field lines can "disconnect" and "reconnect." Given these ambiguities inherent in the magnetic field line formalism, here we avoid committing to a focus on the trajectory of the magnetic field integral curves, and instead prefer to consider an intrinsic geometric parameter: curvature that completely determines a curve in 2D space.

The curvature κ, measuring how rapidly a curve changes direction in space, is defined as

$$\kappa = \|\boldsymbol{b} \cdot \nabla \boldsymbol{b}\|, \tag{1}$$

where $\boldsymbol{b} = \boldsymbol{B}/\|\boldsymbol{B}\|$. The curvature of magnetic field lines is related directly to the curvature drift of the motion of charged particles, which is invoked in certain particle acceleration mechanisms, e.g., first-order Fermi mechanism in magnetic reconnection.[6,7] Indeed, rapid advances in computations and observations have improved the understanding of several features of magnetic reconnection[7–11] that might contribute to particle energization. For example, the curvature drift mechanism (related to the first-order Fermi mechanism) has been identified as the dominant source of particle acceleration.[12–20] One might reason in a qualitative sense: we think of bent field lines as elastic bands under tension, exerting a force ($\sim \kappa B^2$) on the fluid. This force will drive flows as the lines straighten out. It is natural then to inquire the extent to which the curvature drift acceleration and the curvature field are spatially and quantitatively correlated.

Although there is hardly any doubt that the curvature, as an essential feature of the geometrical behavior of magnetic field lines, is a key ingredient in certain particle acceleration mechanisms, the detailed properties of the magnetic field curvature is neither well known nor well understood for a general configuration. The study presented in

this letter addresses this problem by employing numerical simulations of magnetohydrodynamic (MHD) turbulence, with the goal of providing a better physical interpretation of curvature drift acceleration. We find that an intense curvature and a small magnetic field are preferentially colocated. An intense curvature tends to be linearly anticorrelated with the square of magnetic magnitude. Therefore, magnetic energy release via the curvature drift term is in strong association with the curvature field. This result provides new insights into the literature on particle energization during magnetic reconnection, and also favors the influence of turbulent magnetic effects on heating.

II. METHOD

We consider two-dimensional incompressible MHD turbulence. The dynamical equations read

$$\frac{\partial \omega}{\partial t} + (\boldsymbol{v} \cdot \nabla)\omega = (\boldsymbol{B} \cdot \nabla)j + \nu \nabla^2 \omega, \tag{2}$$

$$\frac{\partial a}{\partial t} + (\boldsymbol{v} \cdot \nabla)a = \eta \nabla^2 a, \tag{3}$$

where $\boldsymbol{v}$ is the velocity field, $\omega = (\nabla \times \boldsymbol{v}) \cdot \hat{\boldsymbol{z}}$ is the vorticity, a is the magnetic potential, $\boldsymbol{B} = \nabla a \times \hat{\boldsymbol{z}}$ is the magnetic field, and $j = (\nabla \times \boldsymbol{B}) \cdot \hat{\boldsymbol{z}} = -\nabla^2 a$ is the electric current density. For simplicity, the viscosity ν and resistivity η are set to equal values. The numerical simulation is done with a Fourier spectral method[21] in a doubly periodic $(2\pi)^2$ Cartesian domain with a 8192^2 resolution. The fields are initialized at modes $5 \leq |\boldsymbol{k}| \leq 20$ with random phases and fluctuation amplitudes, whose spectra are proportional to $1/[1 + (k/k_0)^{8/3}]$ with $k_0 = 10$. The total kinetic and magnetic energy are each initially equal to 0.5. We fix $\nu = \eta = 5 \times 10^{-5}$, which corresponds to a high Reynolds number. We carry out our analysis on snapshots near the time of the maximum mean square electric current density.

III. ANTICORRELATION BETWEEN THE CURVATURE AND MAGNETIC FIELD

Curvature is a well-studied geometric characteristic of particle trajectories, its statistical properties having been reported in numerous hydrodynamic turbulence studies.[22–28] Particle trajectories are manifestly different from magnetic field lines, but similar analysis methods are useful to study both cases. As a first step, we compute the probability distribution function (PDF) of the field line curvature in the above-described MHD simulation. The results, shown in Fig. 1, reveal properties that are surprisingly reminiscent of the hydrodynamic particle trajectory case. The distribution is broad and exhibits two clear power-law regimes—a low-curvature plateau scaling as $\sim\kappa^0$, while, the distribution of large curvatures scales as $\sim\kappa^{-2}$.

The physical origins of this feature become more apparent when we rewrite the Lorentz force in terms of $\boldsymbol{B}$, $\boldsymbol{j} \times \boldsymbol{B} = \boldsymbol{B} \cdot \nabla \boldsymbol{B} - \nabla(\boldsymbol{B}^2/2)$, where the second term acts in the same way as the pressure force and the first term is equivalent to $\nabla \cdot (\boldsymbol{B}\boldsymbol{B})$, which can be interpreted as the effect of the surface stress $B_i B_j$ on fluids. Then, we rewrite the force $\boldsymbol{B} \cdot \nabla \boldsymbol{B}$ in terms of curvilinear coordinates attached to a field line

$$\boldsymbol{B} \cdot \nabla \boldsymbol{B} = B \frac{\partial B}{\partial s} \boldsymbol{t} - \frac{B^2}{R} \boldsymbol{n}. \tag{4}$$

Here $B = \|\boldsymbol{B}\|$, s is a coordinate along the field line, $\boldsymbol{t} = \boldsymbol{b}$ and $\boldsymbol{n}$ are unit vectors in the tangential and normal directions, respectively, and
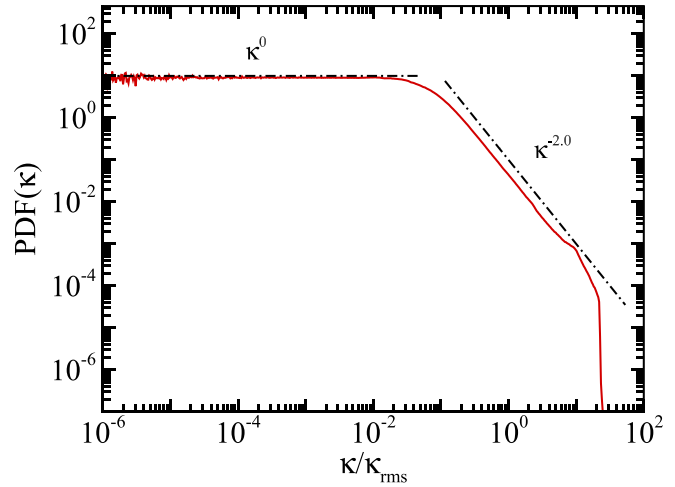
FIG. 1. PDF of the magnetic field curvature κ normalized to the root mean square value κ_{rms}. The PDF has a κ^0 low-curvature regime and a κ^{-2} high-curvature tail.

$R = 1/\kappa$ is the local field line radius. It follows that the curvature can be expressed as

$$\kappa = \frac{\|\boldsymbol{b} \times (\boldsymbol{B} \cdot \nabla \boldsymbol{B})\|}{B^2} = \frac{f_n}{B^2}. \tag{5}$$

According to Eq. (5), one might expect that a large normal force f_n and a small magnetic field both correspond to a high curvature. However, from the joint PDFs in Fig. 2, one can see that the high curvature is not strongly correlated with a large normal force but instead is well associated with a small magnetic field magnitude, while a low curvature is correlated with a small normal force. At a heuristic level, a strong magnetic field may be expected to resist bending. A more specific explanation attributes this anticorrelation between κ and B^2 to the action of the force component normal to the magnetic field line. A large normal force tends to rapidly straighten out the line being in tension, which seems to rule out the possibility of a joint presence of a high curvature and a large magnetic field.

By locating the small and large values of the curvature field, values $\kappa/\kappa_{rms} < 0.01$ and $\kappa/\kappa_{rms} > 0.2$ are plotted on the top of the color map of magnetic magnitude in Fig. 3, which correspond to the κ^0 low-curvature and κ^{-2} high-curvature tails shown in Fig. 1, respectively. No qualitative associations between the low curvature and large magnetic magnitude have been observed in Fig. 3(a), while we can readily identify the concentration of high curvature in regions of low magnetic magnitude in Fig. 3(b). These regions of low magnetic field strength are organized into twisted lines and isolated points. The solitary points are visually found in the vicinity of magnetic island cores, where the direction of the magnetic field changes significantly, leading to a high curvature. The high-curvature lines are preferentially in the form of sheet-like structures around the rims of islands, reminiscent of the well-studied configuration of sheets of electric current density. It is likely, of course, that this association is also related to potential sites of magnetic reconnection.[1]

Based on the above results, we expect that the large-curvature (i.e., $\kappa \to \infty$) and small-curvature (i.e., $\kappa \to 0$) regimes in Fig. 1 should be determined by the scaling behavior of $1/B^2$ as $B \to 0$ and f_n
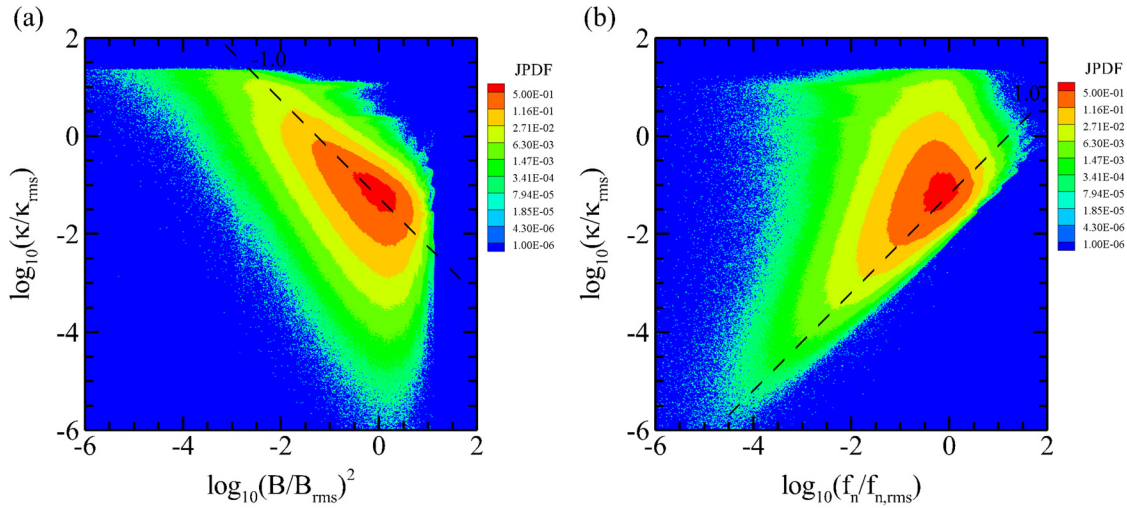
FIG. 2. Joint PDFs of the curvature κ and (a) the square of magnetic magnitude B^2 and (b) the force magnitude f_n acting normal to the field lines. All quantities are normalized to their respective root mean square values. There are apparent associations between the high curvature and low magnetic field and between the low curvature and low normal force.

as $f_n \to 0$, respectively. To make these connections, one may begin by recalling that the x and y components of magnetic fluctuations are independent in isotropic MHD turbulence, and have quasi-Gaussian distributions. The square of magnetic magnitude $B^2 = B_x^2 + B_y^2$ therefore follows a chi-squared distribution with 2 degrees of freedom, deriving the κ^{-2} high-curvature tail as $B \to 0$ by using Taylor expansion. Continuing, suppose we assume that the force f_n at low values is a quasi-Gaussian random variable, recognizing that it could deviate from the Gaussian distribution at high values due to intermittency. Then, the κ^0 low-curvature tail is recovered as $f_n \to 0$.

IV. CURVATURE DRIFT ACCELERATION

The discovery of the anticorrelation between the curvature and magnetic fields is particularly suggestive of some generalizable physical process, such as curvature drift acceleration. From Faraday's law, one readily finds the equation governing magnetic energy $E^m = B^2/2$

$$\frac{\partial E^m}{\partial t} + \nabla \cdot (E \times B) = -E \cdot j, \tag{6}$$

wherein $E \cdot j = E \cdot j_\parallel + E \cdot j_\perp$, and $(\cdots)_\parallel$ and $(\cdots)_\perp$ are quantities parallel and perpendicular with respect to the local magnetic field direction. The perpendicular one can be further decomposed as
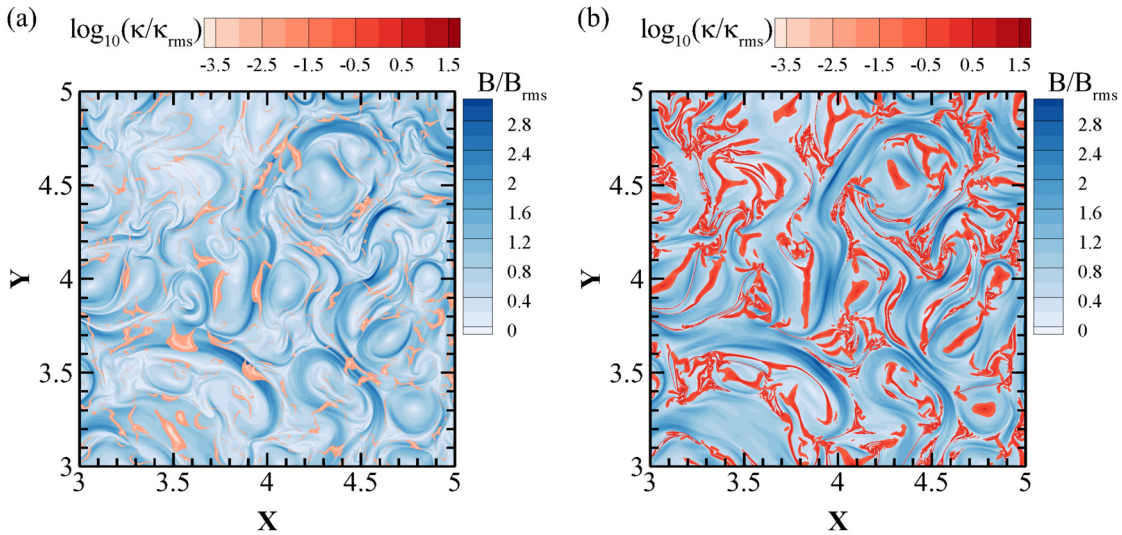

FIG. 3. Contour maps of curvature superposed on the color map of magnetic magnitude in a subregion of the whole domain. (a) Only $\kappa/\kappa_{rms} < 0.01$ values are pictured, and (b) only $\kappa/\kappa_{rms} > 0.2$ values are pictured. The high curvature populates in regions of low magnetic field.

$E \cdot j_\perp = E \cdot \left[\frac{B \times (B \cdot \nabla)B}{B^2}\right] - \nabla\left(\frac{B^2}{2}\right) \cdot \frac{E \times B}{B^2}$, where the second term on the right-hand side can be combined with the second term on the left-hand side in Eq. (6). The remaining term due to the curvature drift, which is reminiscent of the energy conversion rate between the magnetic and kinetic energies,[20] is

$$E \cdot j_c = E \cdot \left[\frac{B \times (B \cdot \nabla)B}{B^2}\right] \sim \kappa B E_\perp, \tag{7}$$

where j_c is the electric current density due to the curvature drift.

The spatial distributions of the curvature drift acceleration term $E \cdot j_c$ [see Fig. 4(a)] and the curvature-related component κB [see Fig. 4(b)] behave quite similarly over the whole domain, apart from regions in the proximity of some special points like magnetic island cores marked as green circles. Instead, the curvature drift acceleration term $E \cdot j_c$ [see Fig. 4(a)] and the perpendicular electric field $E_\perp$ [see Fig. 4(c)] exhibit similarity near these special points (marked as green circles), e.g., both $|E \cdot j_c|$ and $|E_\perp|$ are vanishingly small therein. Here,

we apply the method,[29] examining the topography of magnetic potential, to find O-points (magnetic island cores marked as green circles in Fig. 4) and X-points (magnetic reconnection sites) in 2D. The electric field from Ohm's law $E = -v \times B + \eta j$ is dominated globally by the term $v \times B$,[29] and which is $E = \eta j$ at magnetic island cores and reconnection sites since the magnetic field vanishes at these positions. Therefore, the perpendicular electric field near these special points is very small.

The linear anticorrelation between the curvature and the square of the magnetic field provides a plausible rationale for the similar patterns of κB and κ in Figs. 4(b) and 4(d), where here we also exclude from consideration some special points like magnetic island cores (marked as green circles). Although near magnetic island cores, the direction of the magnetic field changes over very short length scales, corresponding to the intense curvature [e.g., high curvature at the green circles in Fig. 4(d)], the product κB is not typically a local maxima at those positions. This seems to be in apparent contradiction to
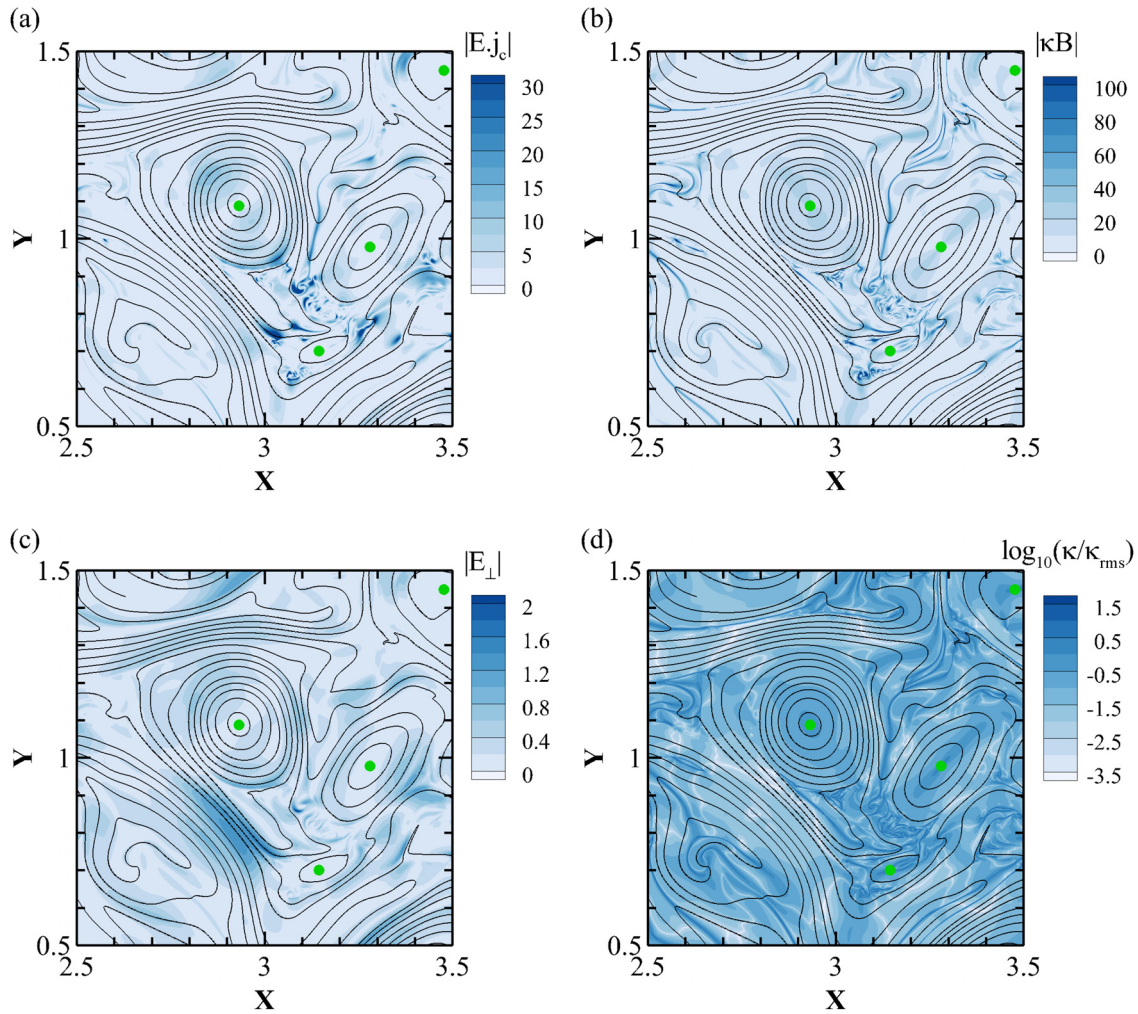

FIG. 4. Contour maps of (a) the curvature drift acceleration term $|E \cdot j_c|$, (b) the curvature-related component $|\kappa B|$, (c) the perpendicular electric field $|E_\perp|$, and (d) the logarithm of the curvature κ in a subregion of the whole domain with the black contour lines showing the magnetic field lines and the green circles representing magnetic island cores.

the preceding description of the general trend, that is, the linear anti-correlation between the curvature and the square of magnetic field leads to κB in an approximately linear relationship with $\sqrt{\kappa}$. However, the measurement of curvature is inevitably limited by the numerical resolution of the simulation. In order to illustrate the effect of grid resolution, we apply a Fourier zero-padding and interpolation technique[29] to obtain a $16\,384^2$ array in place of the original 8192^2 array. One can see from Fig. 5(a) that the Fourier zero-padding and the interpolation technique improve the accuracy of our measurements of curvature and higher resolution enables resolution of a more intense curvature. Also noteworthy from Fig. 5(b) is that the conditional averages of κ tend to form a plateau as the magnetic field vanishes, which could be near magnetic island cores and reconnection sites. It is not possible to numerically measure the true curvature therein since there will always be noise as approaching these zero-magnetic positions.

Previous studies[12–19] on magnetic reconnection emphasize the prominence of curvature drift acceleration in reconnection exhausts, at ends of contracting magnetic islands and in island merging regions. The importance of this process also emerges by virtue of the curvature analysis here. Figures 6(a) and 6(b) show the spatial distributions of the curvature drift acceleration in several subregions including magnetic island cores (marked as green circles) and magnetic reconnection sites (marked as green stars). On the one hand, the curvature drift acceleration at magnetic island cores and reconnection sites is small, as we have shown, due to the negligible perpendicular electric field $E_\perp$ therein. On the other hand, an intense curvature is often found in the vicinity of these positions, thus enhancing the curvature drift acceleration nearby.

The analyses we make so far make no specific reference to turbulence. But turbulence and heating processes related to turbulence are frequently implicated in the study of space and astrophysical plasmas.[30–35] Evidently, turbulence, contemporaneous with magnetic reconnection, operates cooperatively in the natural evolution of the magnetic field in these plasmas.[36–41] Local flows in turbulence, even though they do not contain a magnetic island core or a reconnection site, may also produce a large curvature. To isolate the effect of turbulence, we show subregions where no topologically special points are contained in Figs. 6(c) and 6(d). In comparison with the regions in the

proximity of magnetic reconnection sites and magnetic island cores, the observable enhancement of the curvature drift acceleration emerges as well in turbulence-dominant regions, supporting the view that turbulent effects are playing an essential role in particle acceleration. This point is supported by the results in Ref. 20 as well.

V. FURTHER APPLICATIONS

In this section, we discuss the properties of magnetic field curvature in two different systems that deviate from the statistically homogeneous, isotropic and two-dimensional MHD: isotropic 3D MHD and 2.5D kinetic plasma.

A. 3D MHD

The incompressible three-dimensional MHD equations read

$$\frac{\partial \boldsymbol{v}}{\partial t} + \boldsymbol{v} \cdot \nabla \boldsymbol{v} = -\nabla p^* + \boldsymbol{B} \cdot \nabla \boldsymbol{B} + \nu \nabla^2 \boldsymbol{v}, \tag{8}$$

$$\frac{\partial \boldsymbol{B}}{\partial t} + \boldsymbol{v} \cdot \nabla \boldsymbol{B} = \boldsymbol{B} \cdot \nabla \boldsymbol{v} + \eta \nabla^2 \boldsymbol{B}, \tag{9}$$

where p^* is the total (kinetic + magnetic) pressure, along with $\nabla \cdot \boldsymbol{v} = \nabla \cdot \boldsymbol{B} = 0$. We solve the Fourier-space version of the above equations via a Galerkin spectral method,[42] with 1024 Fourier modes in each spatial direction. For simplicity, equal viscosity and resistivity $\nu = \eta = 4 \times 10^{-4}$ are used. The run is a freely decaying problem in a periodic cube of size 2π and has the initially unity fluctuation energy equipartitioned between the kinetic and magnetic components, i.e., $E_v = E_b = 0.5$. The fields are initialized at modes $1 \le |\boldsymbol{k}| \le 5$ with random phases and fluctuation amplitudes, whose spectra are proportional to $1/[1 + (k/k_0)^{11/3}]$ with $k_0 = 3$. The cross-helicity is always small. We carry out our analysis on a snapshot near the time of maximum mean square current density.

One can see from Fig. 7 that the PDF of the curvature exhibits power laws for both a small-curvature and large-curvature regimes: for a small curvature, the PDF is close to linear with κ, while, for a large curvature, it scales as $\kappa^{-2.5}$. Since dimensonality does not enter into the expression in Eq. (5), we expect that the anticorrelation between the curvature and magnetic field will hold also in a 3D system. This expectation is confirmed in our simulation, see Fig. 8, which shows
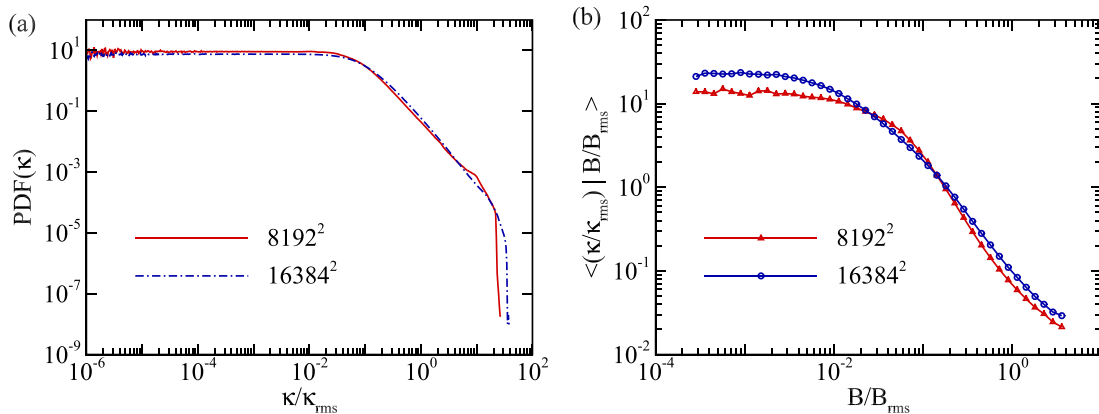

FIG. 5. Comparison between 8192^2 resolution and $16\,384^2$ resolution: (a) PDF of the magnetic field curvature κ and (b) average of the magnetic field curvature κ conditioned on the magnetic magnitude.
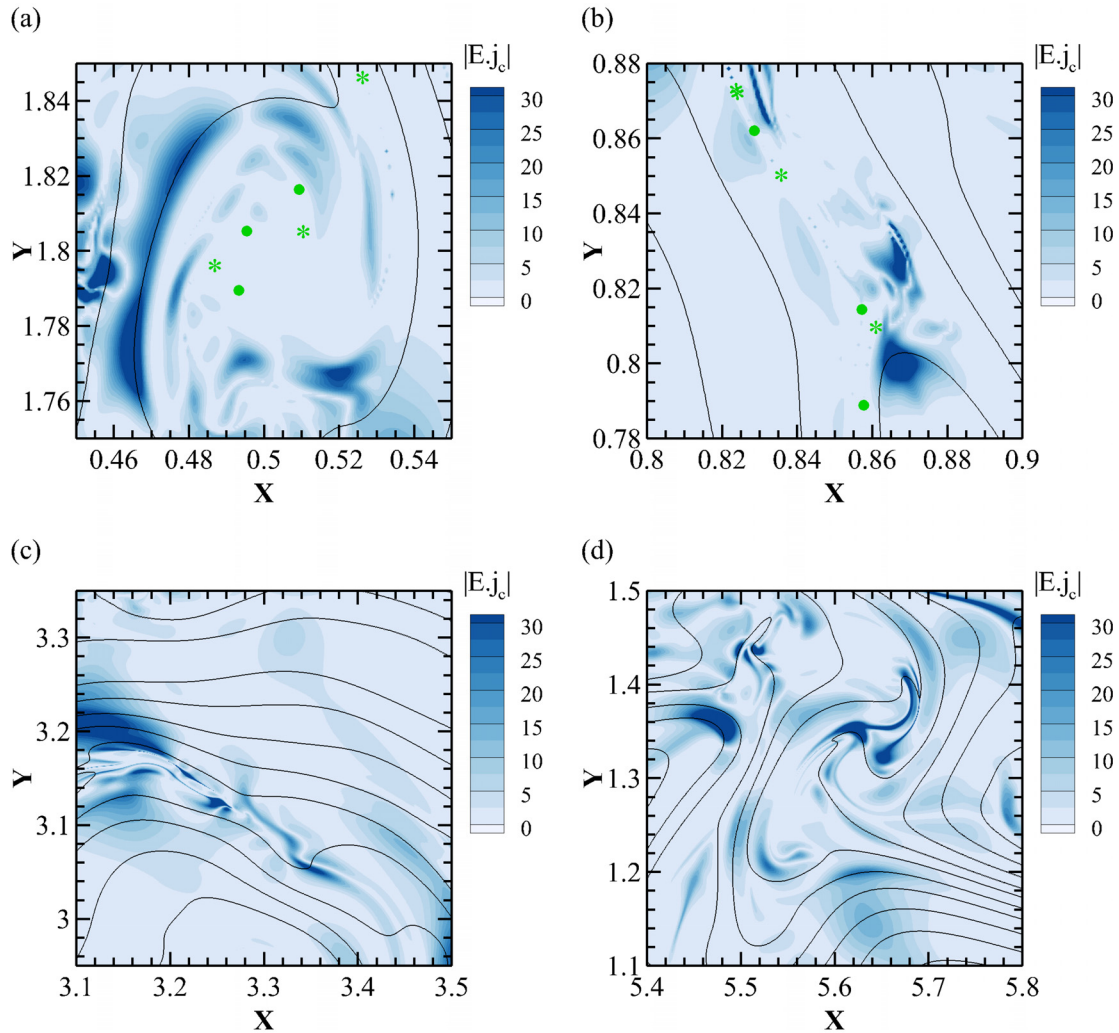
FIG. 6. Contour maps of the curvature drift acceleration term $|E \cdot j_c|$. (a) and (b) Subregions including magnetic island cores (marked as green circles) and magnetic reconnection sites (marked as green stars). (c) and (d) Subregions that do not contain topologically special points. The black contour lines show magnetic field lines.

that a low and high curvature are strongly correlated with a small normal force and a small magnetic field magnitude, respectively. In analogy with the procedure in 2D, the square of magnetic magnitude B^2 in 3D MHD should then be distributed following a chi-squared distribution with 3 degrees of freedom. Since the curvature as $\kappa \to \infty$ scales like B^{-2} as $B^2 \to 0$, one can derive the scaling $P(\kappa) \sim \kappa^{-2.5}$ for a high curvature. A similar reasoning is applicable to the low-curvature regime. Note that the force f_n is confined to the plane orthogonal to the magnetic field. We then assume the PDF of f_n^2 at small values is a chi-squared distribution with 2 degrees of freedom. As $f_n \to 0$, $P(f_n) \sim f_n$, and we recover $P(\kappa) \sim \kappa^1$ for a low curvature.

B. Kinetic plasma

Plasma turbulence involves structures across a wide range of scales, spanning from macroscopic fluid scales to subelectron scales.

Based on what plasma properties we are interested in studying, a plasma can be treated as tractable models in various limits. The MHD model remains a credible approximation for a plasma at scales large enough to be well separated from the kinetic effects, while a more refined kinetic description is required at kinetic scales. Here, we compare the results from fully kinetic particle-in-cell (PIC) simulations with those from MHD simulations.

We employ a fully kinetic simulation by P3D[43] in a 2.5D geometry (three components of dependent field vectors and a two-dimensional spatial grid). The number density is normalized to a reference number density n_r (=1 in this simulation), mass to proton mass m_i (=1 in this simulation), charge to proton charge q_i, and magnetic field to a reference B_r (=1 in this run). The length is normalized to the ion inertial length d_i, time to the ion cyclotron time Ω_i^{-1}, velocity to the reference Alfvén speed $v_{Ar} = B_r/(4\pi m_i n_r)^{1/2}$, and temperature to $T_r = m_i v_{Ar}^2$. The simulation was performed in a periodic domain,
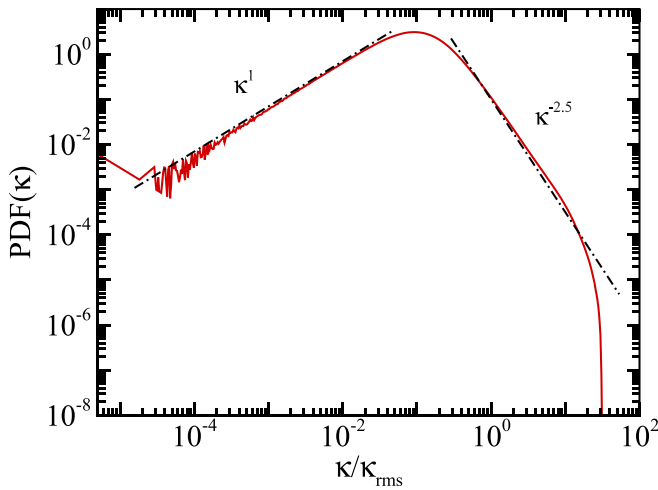
FIG. 7. 3D MHD simulation: PDF of the magnetic field curvature κ normalized to the root mean square value κ_{rms}. The PDF has a κ^1 low-curvature regime and a $\kappa^{-2.5}$ high-curvature tail.
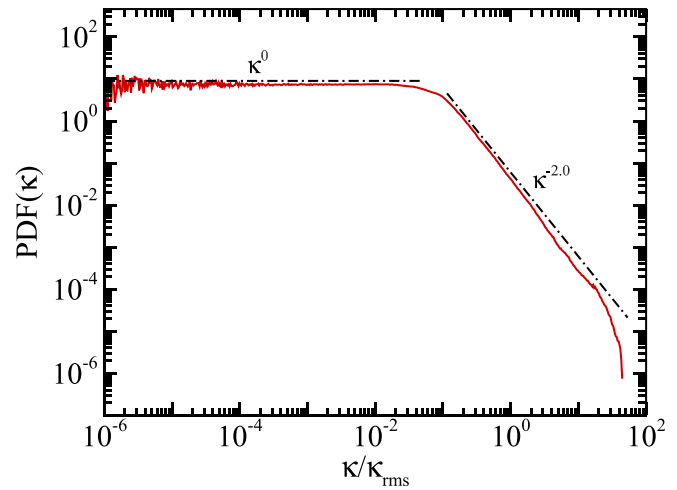

FIG. 9. PIC simulation: PDF of the magnetic field curvature κ normalized to the root mean square value κ_{rms}.

whose size is $L = 150 d_i$, with 4096^2 grid points and 3200 particles of each species per cell ($\sim 107 \times 10^9$ total particles). The ion to electron mass ratio is $m_i/m_e = 25$, and the speed of light in the simulation is $c = 15 v_{Ar}$. The run is a decaying initial value problem, starting with a uniform density ($n_0 = 1.0$) and temperature of ions and electrons ($T_0 = 0.3$). The uniform magnetic field is $B_0 = 1.0$ directed out of the plane. More details about the simulation can be found in Ref. 35. We analyze the statistics using a snapshot near the time of maximum root mean square electric current density.

One can see from Fig. 9 that the PDF has a κ^0 low-curvature regime and a κ^{-2} high-curvature tail. Figure 10 indicates apparent associations between a high curvature and low magnetic field and

between a low curvature and low normal force. Although the PIC simulation enables the resolution of much smaller scales, the corresponding behavior of curvature is essentially similar to that in 2D MHD. The reasoning advanced in Sec. III might therefore be deemed universal for plasma turbulence.

VI. CONCLUSIONS

Curvature characterizes magnetic field lines. For example, both turbulence and magnetic reconnection drive tangled and bent magnetic configurations, corresponding to an intense curvature. We can therefore analyze the curvature properties to improve the understanding of the curvature drift mechanism, often implicated in particle acceleration. In this work, we have clarified the dependence between
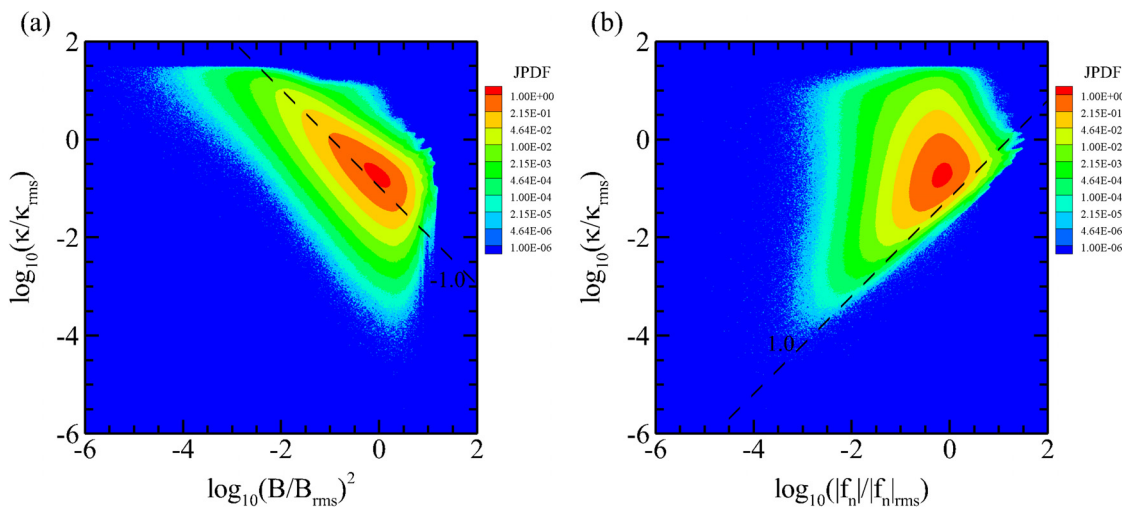

FIG. 8. 3D MHD simulation: joint PDFs of the curvature κ and (a) the square of magnetic magnitude B^2 and (b) the force magnitude f_n acting normal to field lines. All quantities are normalized to their respective root mean square values. There are apparent associations between the high curvature and low magnetic field and between the low curvature and low normal force.
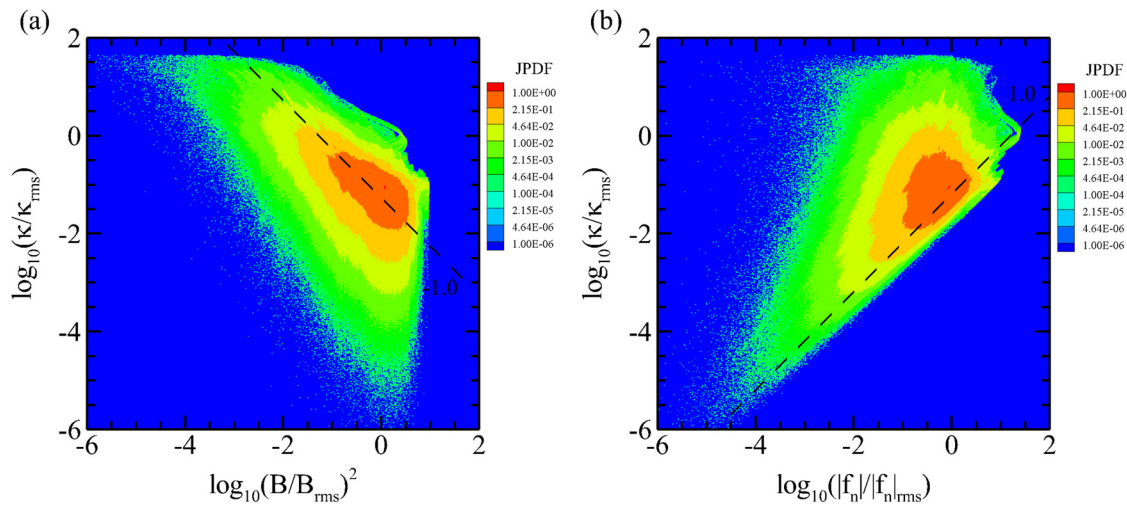
FIG. 10. PIC simulation: joint PDFs of the curvature κ and (a) the square of magnetic magnitude B^2 and (b) the force magnitude f_n acting normal to the field lines.

the high curvature and low magnetic field. In particular, the high curvature κ is statistically scaled as B^{-2}, thus generating the power-law tails of the PDF of curvature. The curvature drift term, responsible for particle energization, is found to be strongly associated with the scalar curvature. It is active in high-curvature positions which could be attributed to turbulence and magnetic reconnection. We have not attempted to quantify the relative strength of these two kinds of acceleration processes here.

The simulations used here include two-dimensional MHD and three-dimensional MHD, but it does not necessarily make a reference to the dimensionality when arriving at Eqs. (5) and (7), in order to maintain as broad a context as possible. It is therefore expected that the relevant statistical features are substantially analogous in 3D and 2D. Indeed, the anticorrelation between a high curvature and low magnetic field applies as well to the 3D case. Also noteworthy is its application for kinetic plasma based on the PIC simulation. However, we should make it clear that this work is neither complete in its coverage nor exhaustive of possibilities. The curvature drift mechanism we study is only one possibility for particle acceleration and other mechanisms have not been addressed herein.

ACKNOWLEDGMENTS

REFERENCES

[1]E. N. Parker, *Cosmical Magnetic Fields: Their Origin and Activity* (Georwdon Press, Oxford, UK, 1979).
[2]W. A. Newcomb, Ann. Phys. **3**, 347 (1958).
[3]J. R. Jokipii, Astrophys. J. **146**, 480 (1966).
[4]J. Jokipii and E. Parker, Astrophys. J. **155**, 777 (1969).
[5]W. Matthaeus, P. Gray, D. Pontius, Jr., and J. Bieber, Phys. Rev. Lett. **75**, 2136 (1995).
[6]T. G. Northrop, Ann. Phys. **15**, 79 (1961).
[7]J. Drake, M. Swisdak, H. Che, and M. Shay, Nature **443**, 553 (2006).
[8]M. Hoshino, T. Mukai, T. Terasawa, and I. Shinohara, J. Geophys. Res.: Space Phys. **106**, 25979, https://doi.org/10.1029/2001JA900052 (2001).
[9]J. Egedal, W. Daughton, and A. Le, Nat. Phys. **8**, 321 (2012).
[10]M. Oka, T.-D. Phan, S. Krucker, M. Fujimoto, and I. Shinohara, Astrophys. J. **714**, 915 (2010).
[11]P. Pritchett, J. Geophys. Res.: Space Phys. **111**, A10212, https://doi.org/10.1029/2006JA011793 (2006).
[12]J. Dahlin, J. Drake, and M. Swisdak, Phys. Plasmas **21**, 092304 (2014).
[13]J. Dahlin, J. Drake, and M. Swisdak, Phys. Plasmas **24**, 092110 (2017).
[14]X. Li, F. Guo, H. Li, and G. Li, Astrophys. J. **843**, 21 (2017).
[15]X. Li, F. Guo, H. Li, and G. Li, Astrophys. J. Lett. **811**, L24 (2015).
[16]F. Guo, H. Li, W. Daughton, and Y.-H. Liu, Phys. Rev. Lett. **113**, 155005 (2014).
[17]Q. Lu, H. Wang, K. Huang, R. Wang, and S. Wang, Phys. Plasmas **25**, 072126 (2018).
[18]H. Wang, Q. Lu, C. Huang, and S. Wang, Astrophys. J. **821**, 84 (2016).
[19]H. Wang, Q. Lu, C. Huang, and S. Wang, Phys. Plasmas **24**, 052113 (2017).
[20]A. Beresnyak and H. Li, Astrophys. J. **819**, 90 (2016).
[21]M. Wan, W. H. Matthaeus, S. Servidio, and S. Oughton, Phys. Plasmas **20**, 042307 (2013).
[22]W. Braun, F. De Lillo, and B. Eckhardt, J. Turbul. **7**, N62 (2006).
[23]H. Xu, N. T. Ouellette, and E. Bodenschatz, Phys. Rev. Lett. **98**, 050201 (2007).
[24]N. T. Ouellette and J. P. Gollub, Phys. Rev. Lett. **99**, 194502 (2007).
[25]N. T. Ouellette and J. P. Gollub, Phys. Fluids **20**, 064104 (2008).
[26]A. Scagliarini, J. Turbul. **12**, N25 (2011).
[27]B. Kadoch, D. del Castillo-Negrete, W. J. Bos, and K. Schneider, Phys. Rev. E **83**, 036314 (2011).
[28]Y. Yang, J. Wang, Y. Shi, Z. Xiao, X. He, and S. Chen, Phys. Rev. Lett. **110**, 064503 (2013).

[29]S. Servidio, W. Matthaeus, M. Shay, P. Dmitruk, P. Cassak, and M. Wan, Phys. Plasmas **17**, 032315 (2010).

[30]P. Dmitruk, W. H. Matthaeus, and N. Seenu, Astrophys. J. **617**, 667 (2004).

[31]J. M. TenBarge and G. G. Howes, Astrophys. J. Lett. **771**, L27 (2013).

[32]S. Perri, M. L. Goldstein, J. C. Dorelli, and F. Sahraoui, Phys. Rev. Lett. **109**, 191101 (2012).

[33]L. Price, M. Swisdak, J. Drake, P. Cassak, J. Dahlin, and R. Ergun, Geophys. Res. Lett. **43**, 6020, https://doi.org/10.1002/2016GL069578 (2016).

[34]R. Bandyopadhyay, A. Chasapis, R. Chhiber, T. Parashar, B. Maruca, W. Matthaeus, S. Schwartz, S. Eriksson, O. Le Contel, H. Breuillard *et al.*, Astrophys. J. **866**, 81 (2018).

[35]Y. Yang, M. Wan, W. H. Matthaeus, L. Sorriso-Valvo, T. N. Parashar, Q. Lu, Y. Shi, and S. Chen, Mon. Not. R. Astron. Soc. **482**, 4933 (2019).

[36]A. Retinò, D. Sundkvist, A. Vaivads, F. Mozer, M. André, and C. J. Owen, Nat. Phys. **3**, 235 (2007).

[37]D. Sundkvist, A. Retinò, A. Vaivads, and S. D. Bale, Phys. Rev. Lett. **99**, 025004 (2007).

[38]W. Matthaeus and M. Velli, Space Sci. Rev. **160**, 145 (2011).

[39]K. Osman, W. Matthaeus, J. Gosling, A. Greco, S. Servidio, B. Hnat, S. C. Chapman, and T. Phan, Phys. Rev. Lett. **112**, 215002 (2014).

[40]V. Zhdankin, D. A. Uzdensky, J. C. Perez, and S. Boldyrev, Astrophys. J. **771**, 124 (2013).

[41]M. Wan, A. F. Rappazzo, W. H. Matthaeus, S. Servidio, and S. Oughton, Astrophys. J. **797**, 63 (2014).

[42]S. A. Orszag and G. Patterson, Jr., Phys. Rev. Lett. **28**, 76 (1972).

[43]A. Zeiler, D. Biskamp, J. F. Drake, B. N. Rogers, M. A. Shay, and M. Scholer, J. Geophys. Res. **107**, 1230, https://doi.org/10.1029/2001JA000287 (2002).